Clinical Kidney Journal, 2025, vol. 18, no. 3, sfaf057

https://doi.org/10.1093/ckj/sfaf057
Advance Access Publication Date: 24 February 2025
Original Article

ORIGINAL ARTICLE

Causal relationships between immune cell phenotypes and primary glomerular diseases: genetic evidence from bidirectional Mendelian randomization study

Wenhao Tang, Qiu Li, Xueying Yang and Haiping Yang

Department of Nephrology Children's Hospital of Chongqing Medical University, Chongqing, China; National Clinical Research Center for Child Health and Disorders, Chongqing, China; Ministry of Education Key Laboratory of Child Development and Disorders, Chongqing, China; Chongqing Key Laboratory of Pediatric Metabolism and Inflammatory Diseases, Chongqing, China

Correspondence to: Haiping Yang; E-mail: oyhp0708@163.com; Xueying Yang; E-mail: xyyang0502@163.com

ABSTRACT

Background. Primary glomerular diseases (PGDs), including nephrotic syndrome (NS), membranous nephropathy (MN), and IgA nephropathy (IgAN), are complex renal conditions influenced by immune system dysregulation. Although associations between immune cell phenotypes and PGDs have been observed, the precise causal relationships have not been fully elucidated.

Methods. Utilizing genetic association data from genome-wide association studies (GWASs), we investigated 731 immunophenotypes in relation to PGDs. A bidirectional two-sample Mendelian randomization (MR) approach, primarily employing inverse variance weighting (IVW), was conducted to establish causality. MR-Egger, weighted median, simple mode, and weighted mode were used as complementary methods to reinforce the robustness and validity of the results. Sensitivity analyses further validated the sensitivity and stability of our results.

Results. We identified 38 immunophenotypes suggestively related to IgAN, with 20 as risk factors and 18 as protective effects. Six immunophenotypes remained significant after Bonferroni correction: The percentage of CD25hi among T cells; the percentage of CD25hi CD45RA$^-$ CD4 not T regulatory (Treg) among T cells; the percentage of CD25hi CD45RA$^-$ CD4 not Treg within the CD4$^+$ T cell population; CX3CR1 expression on monocytes; CD40 expression on monocytes; and CD64 expression on CD14$^+$ CD16$^-$ monocytes. In the validation analysis of IgAN, CD3 expression on effector memory CD4$^+$ T cells further confirmed the predisposing risk role of effector memory T cells in the development of IgAN. Additionally, the MR analysis demonstrated suggestive associations between 25 immunophenotypes and MN (8 risk factors and 17 protective factors), as well as between 22 immunophenotypes and NS (10 risk factors and 12 protective factors). Last, by intersecting the immunophenotypes showing suggestive associations with PGDs, we identified two common immunophenotypes shared by IgAN and MN, three by IgAN and NS, and one by MN and NS.

Conclusions. This genetic-level investigation uncovers causal associations between immunophenotypes and PGDs, providing valuable insights into the immunological underpinnings of PGDs. Our findings suggest potential targets for treatment strategies, thereby facilitating more personalized and effective therapeutic approaches in PGDs management.

Received: 10.10.2024; Editorial decision: 28.1.2025

GRAPHICAL ABSTRACT

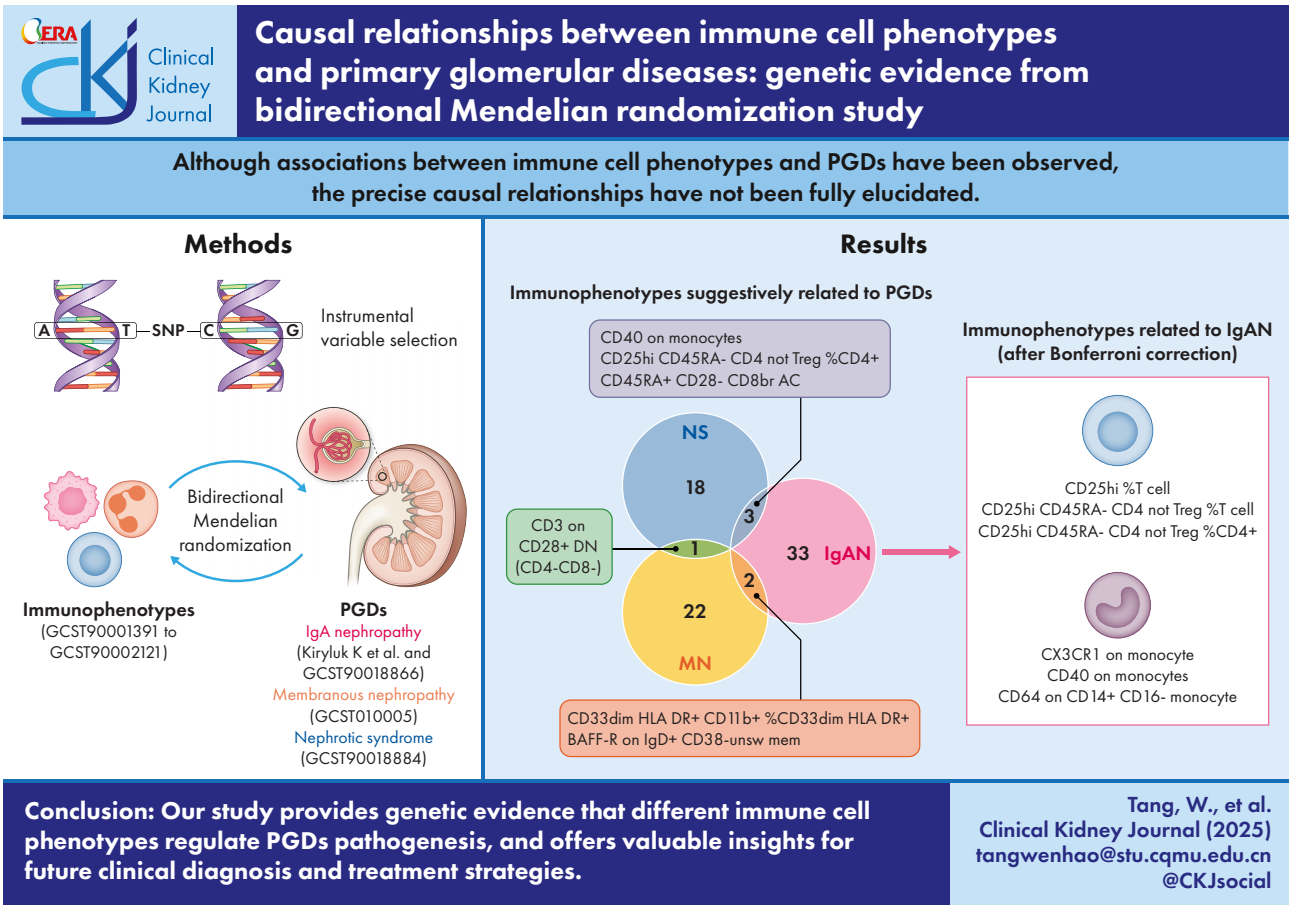

Keywords: immune cell phenotype, Mendelian randomization analysis, primary glomerular diseases

KEY LEARNING POINTS

What was known:

- IgA nephropathy, membranous nephropathy, and nephrotic syndrome are the most common forms of PGDs that represent a significant subset of immune-mediated kidney disorders.
- Multiple studies have highlighted that immune cells play important roles in the progression of PGDs.

This study adds:

- We present direct genetic evidence, highlighting the crucial roles of specific immune cell phenotypes in the pathogenesis of PGDs.
- Our results reflect the fact that immunophenotypes is a more critical initiating factor for IgAN in PGDs.

Potential impact:

- Our research offers invaluable immunological insights for PGDs, paving the way for future early clinical diagnosis and treatment approaches.

INTRODUCTION

Primary glomerular diseases (PGDs) are the leading causes of end-stage renal disease worldwide, necessitating kidney replacement therapy and associated with high morbidity and mortality. This imposes an increasing socioeconomic burden on healthcare systems globally [1, 2]. IgA nephropathy (IgAN), membranous nephropathy (MN), and nephrotic syndrome (NS) are the most common forms of PGD that represent a significant subset of immune-mediated kidney disorders. Despite extensive research, the precise role of the immune system in the pathogenesis of PGDs remains poorly understood.

Immune dysregulation plays a crucial role in the onset and progression of PGDs. For instance, IgAN is characterized by the deposition of IgA-containing immune complexes in the glomeruli, whereas MN is associated with autoantibodies targeting specific podocyte antigens, leading to the immune complex deposition [3, 4]. Notably, the B cell activation factor (BAFF) and A proliferation-inducing ligand (APRIL), which promote B cell differentiation, maturation, and plasma cell antibody secretion, have been implicated in several glomerular diseases [5]. Targeting BAFF/APRIL with specific inhibitors has emerged as a promising therapeutic strategy, with some inhibitors currently in the most advanced stages of clinical validation for IgAN and MN, demonstrating their potential to revolutionize the treatment for this condition [6]. In addition, multiple studies have highlighted the role of adaptive immunity including the imbalance of T cells and innate immunity involving Toll-like receptors and monocytes, in developing PDGs [7–9]. However, the exact pathways through which immune cell phenotypes contribute to the progression of these conditions remain poorly understood. Furthermore, the potential bidirectional interactions between immune responses and glomerular pathology are not well-defined, posing challenges in identifying effective therapeutic targets.

Given these complexities, Mendelian randomization (MR), a rational epidemiological genetic approach, offers a novel perspective for exploring causal relationships between heritable complex traits [10]. Single nucleotide polymorphisms (SNPs) from genome-wide association studies (GWAS) were chosen as instrument variables (IVs) to draw credible causal inferences. Consequently, bias in traditional investigations due to confounding factors and reverse causality can be effectively avoided [11]. In the context of PGDs, bidirectional MR allows for the investigation of both the influence of immune cell phenotypes on the development of NS, IgAN, and MN, and the potential feedback effects of these diseases on immune system modulation.

In this study, we employed bidirectional MR by harnessing GWAS summary statistics from leading consortia to infer and genetically investigate the causal effect between immune cell phenotypes and PGDs. The findings are expected to improve our understanding of the immunopathology of PGDs, informing future strategies for management and treatment.

MATERIALS AND METHODS

Study design

We utilized two-sample MR to evaluate the causal relationships between 731 immunophenotypes and PGDs. The flowchart of the study is shown in Fig. 1. Selecting of appropriate SNPs as instrumental variables (IVs) for causality analysis requires meeting the following criteria: (i) relevance hypothesis: IVs must be strongly associated with the exposure factors; (ii) independence hypothesis: IVs should not be influenced by other confounders; and (iii) exclusionary hypothesis: IVs should affect the outcome factors solely through the exposure factors. All data for this study were sourced from previously published research and public databases, thus eliminating the need for additional ethical approval.

Furthermore, we validated the causal relationships between immunophenotypes and IgAN in an independent cohort. However, due to the lack of available independent datasets for MN and NS, it is currently challenging to perform robust replication for these phenotypes. The process for IgAN validation was consistent with the analysis above.

Data sources

The immunity-wide GWAS of 731 immune cell phenotypes, performed by Valeria Orrù *et al.*, involves a cohort of 3757 Europeans [12]. These 731 immunophenotypes include 118 absolute cell counts (AC), 389 median fluorescence intensities (MFI) reflecting surface antigen levels, 32 morphological parameters (MP), and 192 relative cell counts (RC). The analysis highlighted the characteristics of seven major flow cytometry panels: B cells, cDCs (conventional dendritic cells), mature stage T cells, monocytes, myeloid cells, TBNK (T cells, B cells, natural killer cells), and T regulatory (Treg) cells. GWAS summary statistics for each immunophenotypes are publicly available from the GWAS Catalog (GCST90001391 to GCST90002121).

The genetic variables of PGDs were obtained from publicly available GWASs conducted by each leading consortium. The GWAS analysis for IgAN included 11 European cohorts with 26 734 individuals (5556 cases and 21 178 controls), and the data are available from the Kiryluk Laboratory [13]. The GWAS analysis for the IgAN validation cohort included 477 784 European individuals (15 587 cases and 462 197 controls) [14]. The GWAS analysis for MN included five European cohorts with 7979 individuals (2150 cases and 5829 controls), and for NS included 476 030 European individuals (775 cases and 475 255 controls) [14, 15].

Details on the GWAS summary data sources used in our study are provided in Table 1.

Instrumental variable selection

We applied rigorous filtering procedures to pinpoint robust and reliable instrumental variables (IVs) for MR analysis. First, we selected SNPs that were genome-wide significant ($P < 5 \times 10^{-8}$) for IgAN, IgAN validation, and MN, and suggestive genome-wide significant ($P < 1 \times 10^{-5}$) for immunophenotypes and NS due to its limited significant SNPs. Second, we applied the clumping process with genome linkage disequilibrium in European ancestry ($r^2 < 0.001$, distance threshold >10 000 kb). Proxies based on the correlation ($r^2 > 0.8$) with the original SNPs were used in the reverse but not in the forward MR, considering the number of IVs and the potential bias introduced by proxies [16, 17]. Third, to avoid the impact of weak instrumental variables, we calculated the *F* statistics for all SNPs to assess their strength [18]. Since an *F* value >10 is considered a non-weak instrument, we select SNPs with $F > 10$ for MR analysis. Finally, we removed SNPs that were significantly associated with the outcome ($P < 1 \times 10^{-5}$) to satisfy the exclusionary hypothesis.

Mendelian randomization

All statistical analyses were performed in R v.4.3.1 software. The detailed information on the software, packages, function, and parameters used are provided in Supplementary Table 1. The inverse variance weighted (IVW) method was primarily used to determine the causal relationship between immunophenotypes and PGDs, employing the TwoSampleMR package [19]. IVW was the preferred method for this research since it is the most efficient MR analysis with the highest statistical power, assuming that all SNPs serve as valid instrumental variables without horizontal pleiotropy and thus delivering stable and valid causal estimates [20]. However, due to the difficulty of eliminating horizontal pleiotropy in all SNPs in practical applications, the IVW method is prone to bias, which affects the accuracy of the results. Considering this, the MR-Egger, weighted median,

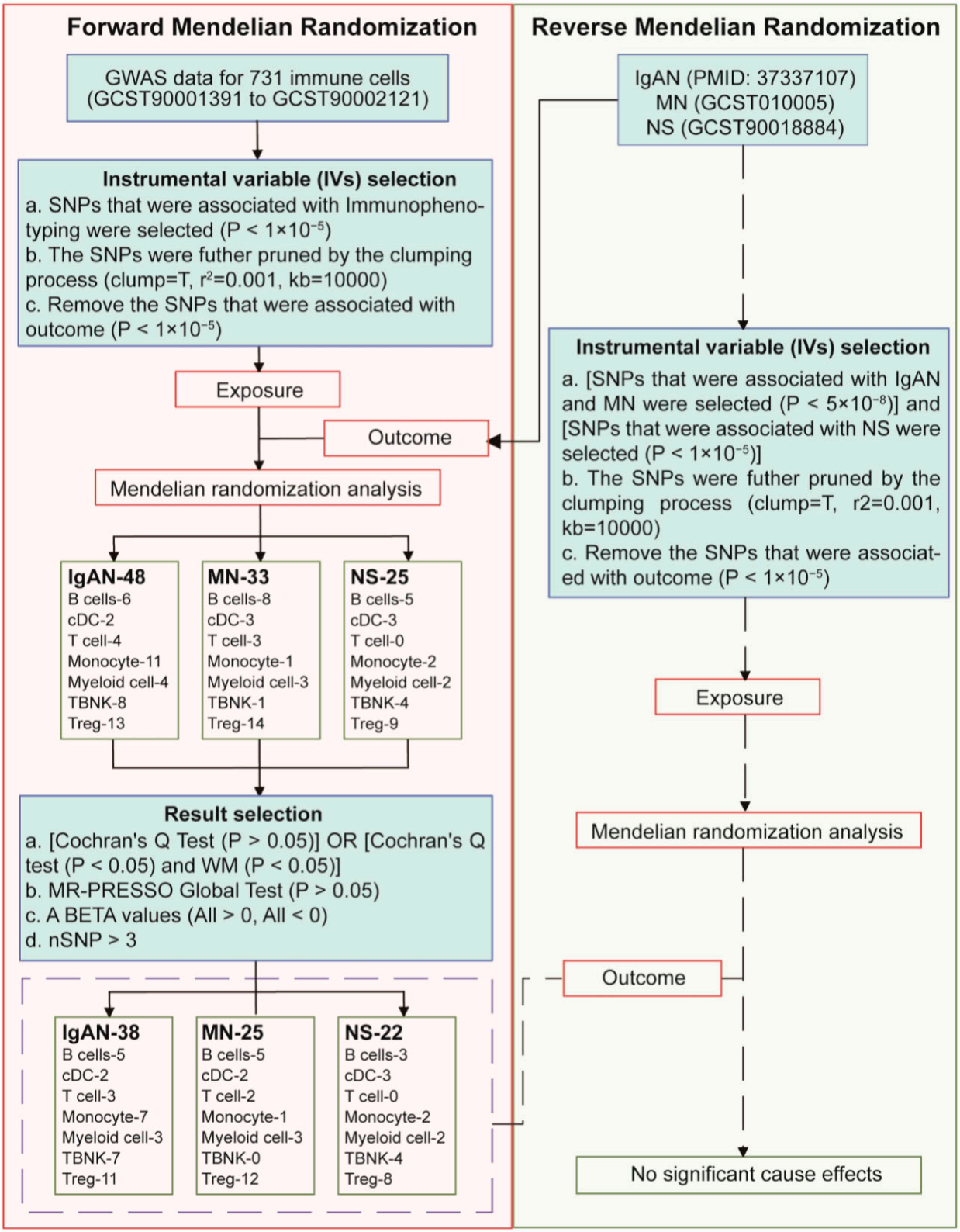

Figure 1: Flowchart of the study. nSNP, number of SNPs.

Table 1: The GWAS data source details in our study.

Phenotype	Data source	Case	Control	Sample size	Ancestry
immunophenotypes	Orrù V *et al.*GCST90001391 to GCST90002121			3 757	European
IgAN	Kiryluk K *et al.*PMID: 37337107	5 556	21 178	26 734	European
IgAN (validation)	Sakaue S *et al.*GCST90018866	15 587	462 197	477 784	European
MN	Xie J *et al.*GCST010005	2 150	5 829	7 979	European
NS	Sakaue S *et al.*GCST90018884	775	475 255	476 030	European

simple mode, and weighted mode were used as complementary methods [21]. Typically, to evaluate the robustness of the results, the heterogeneity of IVW estimates is quantified using Cochran's Q test, with a *P* value below .05 indicating the presence of heterogeneity [22]. However, if the null hypothesis is rejected ($P < .05$), indicating the presence of heterogeneity among SNPs, the results are then evaluated using the weighted median (WM) method [12]. Causal association between the exposure and the outcome is ruled out when the outcomes of the WM method are also found to be non-significant. To mitigate the impact of horizontal pleiotropy, we employed MR-PRESSO to assess its presence and retained the causal inference effects when pleiotropy was not detected, with a *P* value below .05 indicating the presence of horizontal pleiotropy [23]. Besides, we used scatterplots to assess causality, visualize the heterogeneity, and check the impact of outliers. Funnel plots evaluated the heterogeneity of IVs, and leave-one-out analyses examined the potential impact of excluding any IVs on the MR estimates. In the leave-one-out plots, the *P* value for the overall analysis remained below .05 after omitting each SNP, suggesting that no single SNP is disproportionately influencing the results. These methods collectively ensured the sensitivity and stability of the results.

To address multiple testing, we used Bonferroni correction to adjust the *P* value for various immunophenotypes ($P \leq .05/43$ for monocytes, $P \leq .05/190$ for B cells, $P \leq .05/64$ for cDCs, $P \leq .05/64$ for myeloid cells, $P \leq .05/124$ for TBNK cells, $P \leq .05/79$ for maturation stages of T cells, and $P \leq .05/167$ for Treg cells). Causal associations that stayed significant after Bonferroni correction were considered as strong evidence, showing robust significance.

RESULTS

Causal effects between immunophenotypes and IgAN

SNPs were finally selected for IVs based on established filtering procedures. The basic information about the IVs and the corresponding *F* statistics are shown in Supplementary Table 2. As a result, 48 immune cell phenotypes were found to be suggestively associated with IgAN according to IVW methods, as detailed in Supplementary Table 3. Owing to inconsistent effect directions across methods, nine immune phenotypes were excluded. Besides, significant heterogeneity was observed in CD40 expression on $CD14^+$ $CD16^+$ monocytes (Cochran's Q $P = .030$, $WM = .085$) and in the percentage of CD33dim HLA DR^+ $CD11b^+$ within CD33dim HLA DR^+ myeloid cell population (Cochran's Q $P = .040$, $WM = .001$). The latter was retained, considering it suggestively significant in the WM results. No significant horizontal pleiotropy was detected in sensitivity analyses (Supplementary Figs 1–3).

Finally, 38 immunophenotypes were found to be suggestively involved in the pathogenesis of IgAN. Among them, 20 immunophenotypes act as risk factors, while 18 immunophenotypes provide protective effects against IgAN (Fig. 2a). Notably, four immunophenotypes that exert risk effects for IgAN passed the multiple test adjustments of Bonferroni correction: the percentage of CD25hi among T cells ($P^{IVW} = 2.782 \times 10^{-5}$, $OR^{IVW} = 1.324$, $95\%CI^{IVW} = 1.161–1.509$) in the Treg panel, the percentage of CD25hi $CD45RA^-$ CD4 not Treg among T cells ($P^{IVW} = 3.132 \times 10^{-5}$, $OR^{IVW} = 1.205$, $95\%CI^{IVW} = 1.104–1.316$) in the Treg panel, the percentage of CD25hi $CD45RA^-$ CD4 not Treg within $CD4^+$ T cell population ($P^{IVW} = 1.361 \times 10^{-4}$, $OR^{IVW} = 1.193$, $95\%CI^{IVW} = 1.090–1.307$) in the Treg panel, and CX3CR1 expression on monocytes ($P^{IVW} = 8.339 \times 10^{-4}$, $OR^{IVW} = 1.170$, $95\%CI^{IVW} = 1.067–1.283$) in the monocyte panel. Additionally, two immunophenotypes that passed Bonferroni correction exert protective effects against IgAN: CD40 expression on monocytes ($P^{IVW} = 3.134 \times 10^{-4}$, $OR^{IVW} = 0.897$, $95\%CI = 0.846–0.952$) in the monocyte panel and CD64 expression on $CD14^+$ $CD16^-$ monocytes ($P^{IVW} = 5.898 \times 10^{-4}$, $OR^{IVW} = 0.841$, $95\%CI^{IVW} = 0.762–0.928$) in the monocyte panel (Fig. 2b).

Next the causal relationships between immunophenotypes and IgAN were validated in an independent cohort (Supplementary Table 4, Fig. 3a). Five immunophenotypes, which refer to the same subtypes or the same marker and exhibit the same direction, were validated for their causal associations with IgAN (Fig. 3b). Notably, CD3 expression on effector memory $CD4^+$ T cell ($P^{IVW} = 3.524 \times 10^{-4}$, $OR^{IVW} = 1.044$, $95\%CI^{IVW} = 1.020–1.069$), representing the enhanced function of effector memory $CD4^+$ T cells, validated the immunophenotypes of the percentage of CD25hi among T cells, the percentage of CD25hi $CD45RA^-$ CD4 not Treg among T cells and the percentage of CD25hi $CD45RA^-$ CD4 not Treg within $CD4^+$ T cell population. These immunophenotypes are mainly composed of Th1, Th2, and Th17 effector memory cells, and the results confirm that effector memory T cells are a risk factor for IgAN.

Furthermore, we reversed MR analysis to explore whether there was reverse causality between IgAN and the remaining 38 immune cell phenotypes, which resulted in no significant causal effects.

Causal effects between immunophenotypes and MN

A total of 33 immune cell phenotypes with suggestive IVW results showed potential associations with MN (Supplementary Table 5). Eight immune cell phenotypes were excluded due to inconsistent trends in analytical results. The remaining immune cell phenotypes were free of heterogeneity and horizontal pleiotropy (Supplementary Figs 4–6). The final screening identified 25 immune phenotypes, of which eight were risk factors for MN and 17 were protective against MN (Fig. 4a). However, none of the phenotypes passed the threshold after Bonferroni multiple test correction (Fig. 4b).

Subsequently, reverse MR of the remaining 25 immune cell phenotype did not reveal the existence of significant reverse causality for MN.

a

Panel	Trait	Trait type	nSNP	Beta	OR(95% CI)	Pvalue	Bonferroni threshold
B cell	CD19 on CD24+ CD27+	MFI	17	0.127	1.135(1.016 to 1.268)	0.025	
B cell	BAFF–R on IgD+ CD38– unsw mem	MFI	9	−0.114	0.892(0.833 to 0.955)	0.001	
B cell	Sw mem %lymphocyte	RC	15	−0.131	0.877(0.770 to 0.999)	0.049	2.632E−04
B cell	CD19 on IgD− CD38−	MFI	15	−0.202	0.817(0.727 to 0.918)	0.001	
B cell	CD20 on unsw mem	MFI	12	−0.204	0.815(0.707 to 0.940)	0.005	
cDC	CD11c on myeloid DC	MFI	19	0.190	1.209(1.031 to 1.417)	0.019	7.813E−04
cDC	CD11c on granulocyte	MFI	18	−0.140	0.869(0.773 to 0.977)	0.019	
Maturation stages of T cell	Naive DN (CD4−CD8−) %DN	RC	16	0.136	1.145(1.002 to 1.310)	0.047	
Maturation stages of T cell	HVEM on CM CD4+	MFI	13	0.112	1.118(1.036 to 1.207)	0.004	6.329E−04
Maturation stages of T cell	TD DN (CD4−CD8−) %T cell	RC	14	−0.157	0.855(0.755 to 0.968)	0.013	
Monocyte	HLA DR on CD14− CD16+ monocyte	MFI	6	0.171	1.187(1.022 to 1.377)	0.024	
Monocyte	CX3CR1 on monocyte	MFI	15	0.157	1.170(1.067 to 1.283)	8.339E−04*	
Monocyte	CX3CR1 on CD14+ CD16− monocyte	MFI	13	0.114	1.120(1.004 to 1.250)	0.043	
Monocyte	CD40 on CD14+ CD16− monocyte	MFI	12	−0.095	0.909(0.846 to 0.977)	0.009	1.163E−03
Monocyte	CD40 on monocytes	MFI	13	−0.109	0.897(0.846 to 0.952)	3.134E−04*	
Monocyte	CX3CR1 on CD14− CD16−	MFI	9	−0.133	0.875(0.769 to 0.995)	0.042	
Monocyte	CD64 on CD14+ CD16− monocyte	MFI	14	−0.173	0.841(0.762 to 0.928)	5.898E−04*	
Myeloid cell	CD33dim HLA DR+ CD11b+ %CD33dim HLA DR+	RC	15	−0.102	0.903(0.833 to 0.979)	0.014	
Myeloid cell	CD11b on CD14+ monocyte	MFI	16	−0.103	0.902(0.839 to 0.970)	0.005	7.813E−04
Myeloid cell	CD11b on CD33br HLA DR+ CD14dim	MFI	11	−0.146	0.864(0.791 to 0.944)	0.001	
TBNK	CD4+ AC	AC	13	0.264	1.302(1.103 to 1.537)	0.002	
TBNK	CD3− lymphocyte AC	AC	10	0.233	1.263(1.050 to 1.519)	0.013	
TBNK	FSC−A on CD4+	MP	12	0.142	1.153(1.011 to 1.314)	0.033	
TBNK	B cell AC	AC	22	0.119	1.126(1.007 to 1.259)	0.037	4.032E−04
TBNK	CD3 on HLA DR+ CD8br	MFI	16	0.110	1.116(1.007 to 1.237)	0.036	
TBNK	DN (CD4−CD8−) AC	AC	15	−0.186	0.830(0.718 to 0.960)	0.012	
TBNK	CD45 on HLA DR+ CD4+	MFI	9	−0.251	0.778(0.660 to 0.917)	0.003	
Treg	CD25hi %T cell	RC	8	0.280	1.324(1.161 to 1.509)	2.782E−05*	
Treg	CD28− CD127− CD25++ CD8br %T cell	RC	10	0.238	1.268(1.015 to 1.584)	0.036	
Treg	CD25hi CD45RA− CD4 not Treg %T cell	RC	13	0.187	1.205(1.104 to 1.316)	3.132E−05*	
Treg	CD127 on granulocyte	MFI	14	0.186	1.204(1.022 to 1.418)	0.026	
Treg	CD25hi CD45RA− CD4 not Treg %CD4+	RC	12	0.177	1.193(1.090 to 1.307)	1.361E−04*	2.994E−04
Treg	CD4 Treg %T cell	RC	12	0.162	1.176(1.033 to 1.338)	0.014	
Treg	CD127 on CD28− CD8br	MFI	12	0.138	1.148(1.045 to 1.262)	0.004	
Treg	CD45RA+ CD28− CD8br AC	AC	206	6.978E−05	1.000(1.000 to 1.000)	0.048	
Treg	CD127 on CD45RA+ CD4+	MFI	13	−0.154	0.857(0.745 to 0.986)	0.031	
Treg	Activated & resting Treg AC	AC	11	−0.196	0.822(0.699 to 0.967)	0.018	
Treg	CD25 on CD39+ secreting Treg	MFI	12	−0.205	0.815(0.695 to 0.955)	0.011	

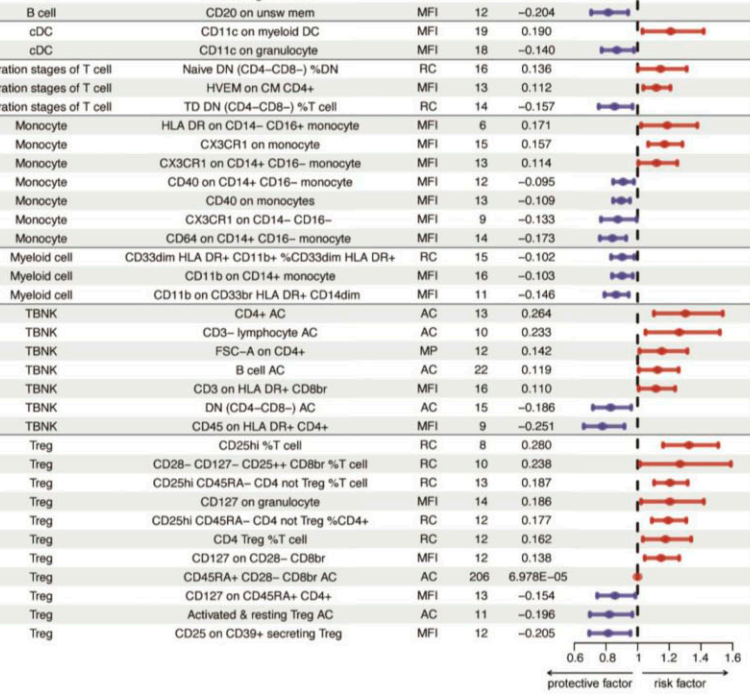

b

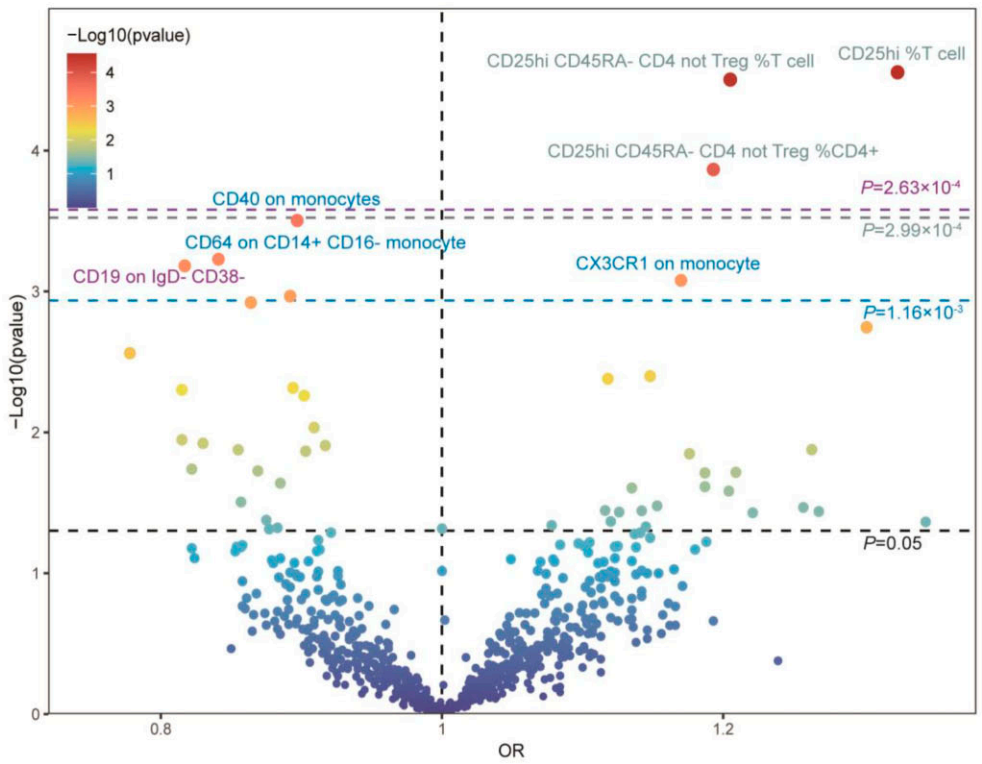

Figure 2: Forest plot and volcano plot indicating IVW analysis results of IgAN. (**a**) Forest plot demonstrating immunophenotypes with a positive causal relationship with IgAN. Beta = ln (OR), expressing as change in ln (OR) of outcome per each additional SD unit of exposure. (**b**) Volcano plots depicting causal associations of 731 immunophenotypes with IgAN. nSNP, number of SNPs; OR, odds ratio; CI, confidence interval.

a

Panel	Trait	Trait type	nSNP	Beta	OR(95% CI)	Pvalue	Bonferroni threshold
B cell	CD24 on IgD− CD38dim	MFI	6	0.051	1.052(1.005 to 1.102)	0.031	
B cell	IgD on transitional	MFI	29	0.036	1.037(1.000 to 1.075)	0.049	2.632E−04
B cell	CD19 on memory B cell	MFI	27	−0.036	0.965(0.934 to 0.997)	0.031	
B cell	IgD− CD38dim AC	AC	16	−0.046	0.955(0.918 to 0.994)	0.023	
cDC	CCR2 on CD62L+ myeloid DC	MFI	15	−0.042	0.958(0.926 to 0.993)	0.018	7.813E−04
Maturation stages of T cell	CD3 on EM CD4+	MFI	18	0.043	1.044(1.020 to 1.069)	3.524E−04*	
Maturation stages of T cell	CD3 on Naive CD4+	MFI	28	0.021	1.021(1.002 to 1.041)	0.032	6.329E−04
Maturation stages of T cell	CD4 on CM CD4 +	MFI	14	−0.060	0.942(0.908 to 0.978)	0.002	
Monocyte	HLA DR on CD14− CD16−	MFI	22	0.026	1.026(1.002 to 1.051)	0.035	1.163E−03
Monocyte	CD14+ CD16+ monocyte %monocyte	RC	26	−0.033	0.968(0.937 to 1.000)	0.05	
TBNK	T cell %lymphocyte	RC	14	0.048	1.049(1.001 to 1.099)	0.044	
TBNK	TCRgd AC	AC	18	0.042	1.043(1.001 to 1.086)	0.043	
TBNK	NKT %lymphocyte	RC	34	0.035	1.036(1.008 to 1.065)	0.012	
TBNK	CD3 on HLA DR+ CD4+	MFI	28	0.034	1.035(1.007 to 1.063)	0.012	4.032E−04
TBNK	CD3 on HLA DR+ T cell	MFI	27	0.032	1.033(1.010 to 1.056)	0.005	
TBNK	HLA DR on HLA DR+ NK	MFI	22	−0.019	0.981(0.963 to 0.999)	0.04	
TBNK	SSC−A on granulocyte	MP	27	−0.033	0.967(0.944 to 0.991)	0.008	
TBNK	HLA DR+ CD4+ %lymphocyte	RC	21	−0.047	0.954(0.919 to 0.990)	0.014	
Treg	CD4 Treg %T cell	RC	16	0.045	1.046(1.008 to 1.085)	0.016	
Treg	CD3 on CD39+ CD8br	MFI	15	0.036	1.037(1.002 to 1.073)	0.038	
Treg	CD3 on CD28+ CD45RA+ CD8br	MFI	24	0.033	1.034(1.007 to 1.062)	0.014	
Treg	CD25 on CD4+	MFI	15	0.027	1.028(1.005 to 1.051)	0.015	2.994E−04
Treg	CD3 on CD39+ CD4+	MFI	28	0.027	1.028(1.004 to 1.052)	0.024	
Treg	CD3 on CD8br	MFI	23	0.025	1.025(1.000 to 1.051)	0.048	
Treg	CD127 on granulocyte	MFI	30	−0.036	0.965(0.932 to 0.998)	0.037	

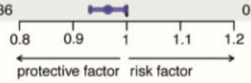

b

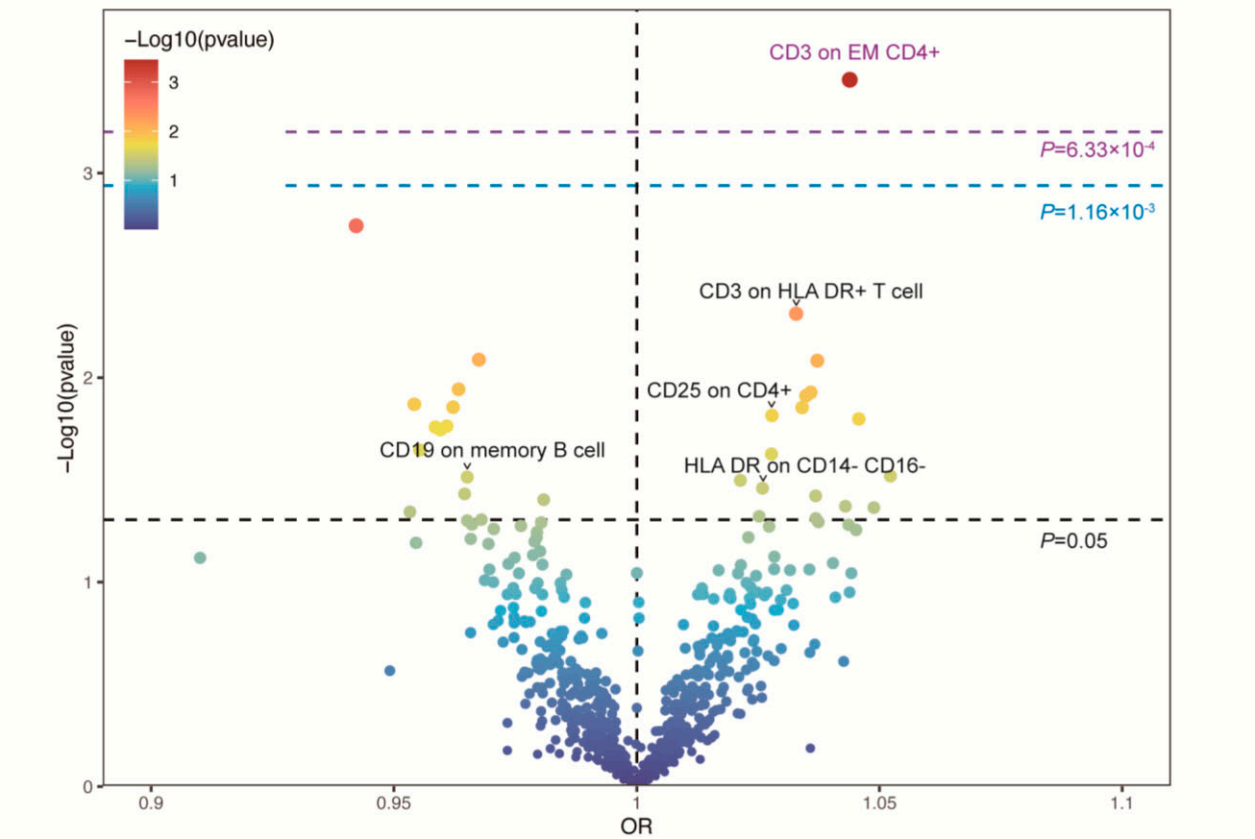

Figure 3: Forest plot and volcano plot indicating IVW analysis results of IgAN validation. (**a**) Forest plot demonstrating immunophenotypes with a positive causal relationship with IgAN validation. Beta = ln (OR), expressing as change in ln (OR) of outcome per each additional SD unit of exposure. (**b**) Volcano plots depicting causal associations of 731 immunophenotypes with IgAN validation. nSNP, number of SNPs; OR, odds ratio; CI, confidence interval.

a

Panel	Trait	Trait type	nSNP	Beta	OR(95% CI)	Pvalue	Bonferroni threshold
B cell	IgD− CD38dim %B cell	RC	9	0.252	1.286(1.002 to 1.652)	0.048	
B cell	BAFF−R on IgD+ CD38− unsw mem	MFI	5	−0.116	0.891(0.801 to 0.990)	0.032	
B cell	BAFF−R on IgD+ CD38dim	MFI	10	−0.118	0.889(0.793 to 0.996)	0.043	2.632E−04
B cell	CD20 on B cell	MFI	14	−0.181	0.835(0.705 to 0.988)	0.036	
B cell	CD19 on IgD+ CD38− unsw mem	MFI	7	−0.229	0.796(0.649 to 0.975)	0.028	
cDC	CD62L− plasmacytoid DC %DC	RC	9	0.233	1.263(1.015 to 1.571)	0.036	7.813E−04
cDC	CD86 on myeloid DC	MFI	5	−0.371	0.690(0.521 to 0.916)	0.010	
Maturation stages of T cell	HVEM on CD4+	MFI	13	−0.135	0.874(0.770 to 0.992)	0.037	6.329E−04
Maturation stages of T cell	EM DN (CD4−CD8−) %T cell	RC	6	−0.296	0.743(0.574 to 0.964)	0.025	
Monocyte	PDL−1 on CD14− CD16−	MFI	9	−0.376	0.687(0.545 to 0.864)	1.377E-03	1.163E−03
Myeloid cell	CD11b on basophil	MFI	9	0.146	1.157(1.011 to 1.325)	0.034	
Myeloid cell	CD11b on CD33dim HLA DR−	MFI	10	0.139	1.149(1.007 to 1.312)	0.040	7.813E−04
Myeloid cell	CD33dim HLA DR+ CD11b+ %CD33dim HLA DR+	RC	9	−0.106	0.899(0.815 to 0.992)	0.034	
Treg	CD127 on CD28+ CD45RA+ CD8br	MFI	5	0.335	1.398(1.051 to 1.861)	0.021	
Treg	CD127 on CD28+ DN (CD4−CD8−)	MFI	9	0.246	1.279(1.018 to 1.607)	0.035	
Treg	CD3 on CD28+ DN (CD4−CD8−)	MFI	5	0.197	1.217(1.015 to 1.460)	0.034	
Treg	CD25 on CD39+ CD4+	MFI	9	0.125	1.133(1.028 to 1.249)	0.012	
Treg	CD45RA+ CD28− CD8br %CD8br	RC	8	−0.016	0.984(0.969 to 1.000)	0.044	
Treg	CD39+ activated Treg %CD4 Treg	RC	7	−0.092	0.912(0.839 to 0.991)	0.030	2.994E−04
Treg	CD3 on CD39+ secreting Treg	MFI	12	−0.123	0.884(0.784 to 0.997)	0.044	
Treg	CD39+ resting Treg %resting Treg	RC	9	−0.125	0.883(0.793 to 0.983)	0.023	
Treg	CD28 on secreting Treg	MFI	10	−0.175	0.840(0.708 to 0.996)	0.044	
Treg	CD28 on CD39+ CD4+	MFI	5	−0.183	0.833(0.736 to 0.943)	0.004	
Treg	CD28 on activated & secreting Treg	MFI	9	−0.216	0.806(0.685 to 0.948)	0.009	
Treg	CD28 on CD39+ activated Treg	MFI	4	−0.248	0.780(0.641 to 0.949)	0.013	

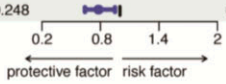

b

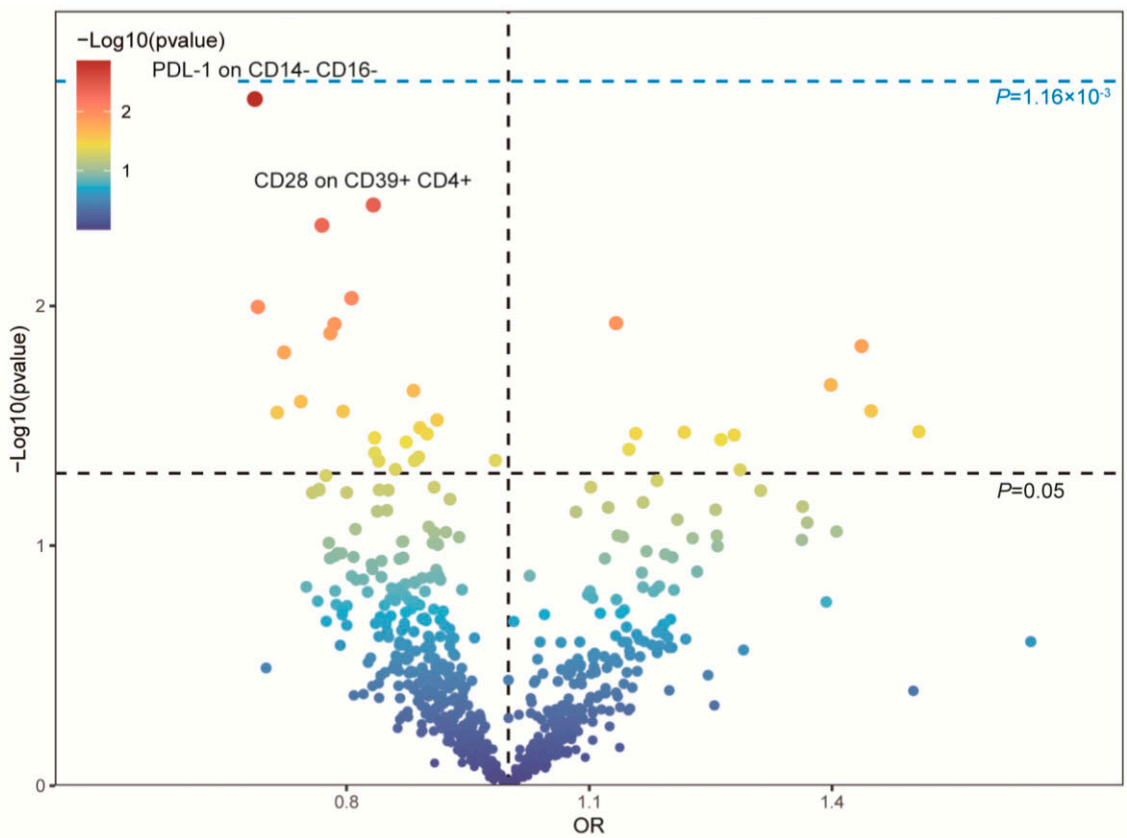

Figure 4: Forest plot and volcano plot indicating IVW analysis results of MN. (**a**) Forest plot demonstrating immunophenotypes with a positive causal relationship with MN. Beta = ln (OR), expressing as change in ln (OR) of outcome per each additional SD unit of exposure. (**b**) Volcano plots depicting causal associations of 731 immunophenotypes with MN. nSNP, number of SNPs; OR, odds ratio; CI, confidence interval.

Causal effect between immunophenotypes and NS

A total of 25 immune cell phenotypes with suggestive IVW results showed potential associations with NS (Supplementary Table 6). The percentage of $CD39^+$ CD8bright within CD8bright T cells (Treg panel); BAFF-R expression on IgD^+ (B cell panel) and CD27 expression on IgD^- CD38dim (B cell panel) were removed due to inconsistent effect directions. No significant heterogeneity or horizontal pleiotropy was detected in sensitivity analyses of the remaining immune cell phenotypes (Supplementary Figs 7–9). The final screen identified 22 immune phenotypes, of which 10 were risk factors for NS and 12 were protective against NS (Fig. 5a). None of the phenotypes passed the threshold after Bonferroni multiple test correction (Fig. 5b).

Afterward, reverse MR analysis suggested that no significant reverse causal relationship existed between the remaining 22 immune cell phenotypes and NS.

Causal analysis of immunophenotypes and PGDs

To explore the immunophenotypes most likely to influence PGDs, we intersected those demonstrating suggestive associations with IgAN, MN, and NS, and constructed Venn diagrams (Fig. 6). BAFF-R expression on IgD^+ $CD38^-$ unswitched memory B cells ($IVW^{IgAN} = 0.001$, $OR^{IgAN} = 0.892$; $IVW^{MN} = 0.032$, $OR^{MN} = 0.891$) in the B cells panel and the percentage of CD33dim HLA DR^+ $CD11b^+$ within the CD33dim HLA DR^+ myeloid cell population ($IVW^{IgAN} = 0.014$, $OR^{IgAN} = 0.903$; $IVW^{MN} = 0.034$, $OR^{MN} = 0.899$) in the myeloid cell panel had causal relationships with protective effects for both IgAN and MN without heterogeneity or horizontal pleiotropy. CD40 expression on monocytes ($IVW^{IgAN} = 3.134 \times 10^{-4}$, $OR^{IgAN} = 0.897$; $IVW^{NS} = 0.039$, $OR^{NS} = 1.052$) in the monocyte panel, the percentage of CD25hi CD45RA$^-$ CD4 not Treg within the $CD4^+$ T cell population ($IVW^{IgAN} = 1.361 \times 10^{-4}$, $OR^{IgAN} = 1.193$; $IVW^{NS} = 0.046$, $OR^{NS} = 1.087$) in the Treg panel, and absolute counts of CD45RA$^+$ CD28$^-$ CD8bright ($IVW^{IgAN} = 0.048$, $IVW^{NS} = 0.031$, $OR^{IgAN} = 1.000$, $OR^{NS} = 1.000$) in the Treg panel exhibited positively causal associations with IgAN and NS without heterogeneity and horizontal pleiotropy. However, the actual risk or protective effects of absolute counts of CD45RA$^+$ CD28$^-$ CD8bright had no clinical significance. Notably, CD40 expression on monocytes had a different impact on IgAN and NS. CD3 expression on CD28$^+$ DN (CD4$^-$CD8$^-$ double negative) ($IVW^{MN} = 0.034$, $OR^{MN} = 1.217$; $IVW^{NS} = 0.023$, $OR^{NS} = 1.129$) in the Treg panel showed causal relationships, and is a risk factor for both NS and MN without heterogeneity or horizontal pleiotropy.

DISCUSSION

To our knowledge, this is the first study to explore the causal relationship between immune cell phenotypes and PGDs using MR analysis. Although Shu *et al*. have investigated the causal roles of immune cell phenotypes in IgAN, the original IgAN GWAS data used are not the most suitable for MR analysis due to the insufficient sample size (592 IgA nephropathy cases), which limits the power for causal characterization [24]. Therefore, our study employed the largest and most up-to-date PGDs GWAS studies to investigate the shared and distinct genetic contributions of immune cell phenotypes to PGDs.

Through a series of MR analyses following strict criteria, we pinpointed immunophenotypes in cDCs, Tregs, B cells, TBNK, maturation stages of T cells, myeloid cells, and monocytes, which were suggestively correlated with PGDs (IgAN = 38, IgAN validation = 25, MN = 25, NS = 22). However, only the causal immunophenotype associations with IgAN reached the Bonferroni adjusted significance, which indicated that immune cells play the most crucial role in the pathogenesis of IgAN in PDGs.

A total of six immunophenotypes demonstrated significant causality for IgAN. Among these, three belong to the Treg panel (the percentage of CD25hi among T cells, the percentage of CD25hi CD45RA$^-$ CD4 not Treg among T cells, and the percentage of CD25hi CD45RA$^-$ CD4 not Treg within $CD4^+$ T cell population), and three belong to the monocyte panel (CD40 expression on monocytes, CD64 expression on $CD14^+$ $CD16^-$ monocytes, and CX3CR1 expression on monocytes). The subsequent validation study, which resulted in the identification of CD3 expression on effector memory $CD4^+$ T cells, further confirmed the predisposing risk role of effector memory T cells in the development of IgAN.

The CD25hi cell population can be divided into Treg and non-Treg cell populations based on CD127 expression, with CD127hi occupying a dominant position [12, 25]. $CD4^+$ CD25hi CD127hi cells are predominantly effector memory T cells, with immunophenotypes of CD25hi CD45RA$^-$ $CD4^+$ not Treg, including Th1, Th2, and Th17 cells [25–27]. Additionally, CD3, an essential T cell marker, forms a non-covalently bound TCR–CD3 complex with the T cell receptor (TCR), which activates the adaptive immune response by binding to peptide-major histocompatibility complex molecules on antigen-presenting cells. This interaction drives T cell proliferation and the production and secretion of effector molecules critical for T cell-mediated immunity [28–30]. Studies demonstrate elevated percentages of effector memory $CD4^+$ T lymphocytes (Th1, Th2, and Th17 cells) in IgAN patients compared to healthy controls [27, 31]. Experiments with lymphocytes from IgAN patients have proved that Th2 cells promote hypogalactosylation of IgA, acting as a risk factor for IgAN. Additionally, Th17 cells produce IL-17, which induces hypermethylation of CpG islands in the C1GALT1C1 gene promoter, leading to the downregulation of C1GALT1C1 mRNA and increased secretion of aberrantly glycosylated IgA1 from B cells [32, 33].

Notably, CD25 (IL-2Rα), which forms the high-affinity IL-2 receptor complex, may serve as an attractive novel target for IgAN therapy based on genetic insights from our research. Currently, tacrolimus has been widely used in the treatment of IgAN by indirectly inhibiting IL-2 production through the suppression of calcineurin activity and the subsequent blocking of NFAT (nuclear factor of activated T cells)-dependent IL-2 transcription. Given this, we propose that monoclonal antibodies directly targeting CD25 could potentially be effective in treating IgAN. Basiliximab, a monoclonal antibody targeting CD25, is currently used in organ transplantation to reduce T cell activity. Studies have shown that Basiliximab effectively reduces IgAN recurrence after kidney transplantation and treats refractory autoimmune encephalitis [34, 35]. Although no studies have specifically explored the direct use of Basiliximab in IgAN treatment, we suggest that it could be a promising therapeutic option for IgAN.

Additionally, the significant immunophenotypes of CD40, CX3CR1 expression on monocytes, and CD64 expression on $CD14^+$ $CD16^-$ monocytes indicates the vital role of monocytes in the pathogenesis of IgAN. Individuals with genetically elevated levels of CD40 expression on monocyte have a significantly lower risk of developing IgAN. According to Orrù's study, CD40 expression on monocytes acts as a protective factor, and activating CD40 may be effective in treating several autoimmune diseases, such as Crohn's Disease, Ankylosing Spondylitis, and

a

Panel	Trait	Trait type	nSNP	Beta	OR(95% CI)	Pvalue	Bonferroni threshold
B cell	CD27 on IgD+ CD24+	MFI	31	−0.082	0.922(0.865 to 0.982)	0.011	
B cell	IgD on IgD+ CD38dim	MFI	21	−0.097	0.908(0.837 to 0.984)	0.019	2.632E−04
B cell	IgD+ %Lymphocyte	RC	18	−0.103	0.902(0.822 to 0.991)	0.031	
cDC	CD62L on granulocyte	MFI	18	0.162	1.175(1.031 to 1.339)	0.015	
cDC	FSC−A on granulocyte	MP	21	0.109	1.116(1.002 to 1.242)	0.045	7.813E−04
cDC	CD62L− HLA DR++ monocyte %monocyte	RC	12	−0.163	0.849(0.743 to 0.972)	0.017	
Monocyte	CD14+ CD16+ monocyte %monocyte	RC	26	0.134	1.143(1.052 to 1.243)	0.002	1.163E−03
Monocyte	CD40 on monocytes	MFI	29	0.051	1.052(1.002 to 1.105)	0.039	
Myeloid cell	CD45 on lymphocyte	MFI	19	−0.102	0.903(0.815 to 0.999)	0.049	7.813E−04
Myeloid cell	CD45 on Im MDSC	MFI	11	−0.109	0.897(0.820 to 0.981)	0.017	
TBNK	CD8br %leukocyte	RC	15	0.145	1.156(1.007 to 1.326)	0.039	
TBNK	FSC−A on lymphocyte	MP	16	0.128	1.136(1.012 to 1.275)	0.030	4.032E−04
TBNK	NKT AC	AC	34	0.07	1.073(1.004 to 1.147)	0.039	
TBNK	CD8 on CD8br	MFI	29	−0.112	0.894(0.824 to 0.970)	0.007	
Treg	CD3 on CD28+ DN (CD4−CD8−)	MFI	15	0.121	1.129(1.017 to 1.253)	0.023	
Treg	CD39 on CD39+ CD8br	MFI	24	0.09	1.094(1.001 to 1.195)	0.048	
Treg	CD25hi CD45RA− CD4 not Treg %CD4+	RC	23	0.083	1.087(1.002 to 1.179)	0.046	
Treg	CD45RA+ CD28− CD8br AC	AC	718	−2.947E−05	1.000(1.000 to 1.000)	0.031	2.994E−04
Treg	CD28+ CD45RA+ CD8dim %T cell	RC	37	−0.036	0.965(0.932 to 0.998)	0.039	
Treg	CD39+ resting Treg AC	AC	28	−0.098	0.906(0.839 to 0.979)	0.012	
Treg	CD28− DN (CD4−CD8−) AC	AC	29	−0.11	0.896(0.808 to 0.993)	0.036	
Treg	CD127 on T cell	MFI	17	−0.14	0.869(0.773 to 0.978)	0.020	

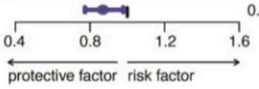

b

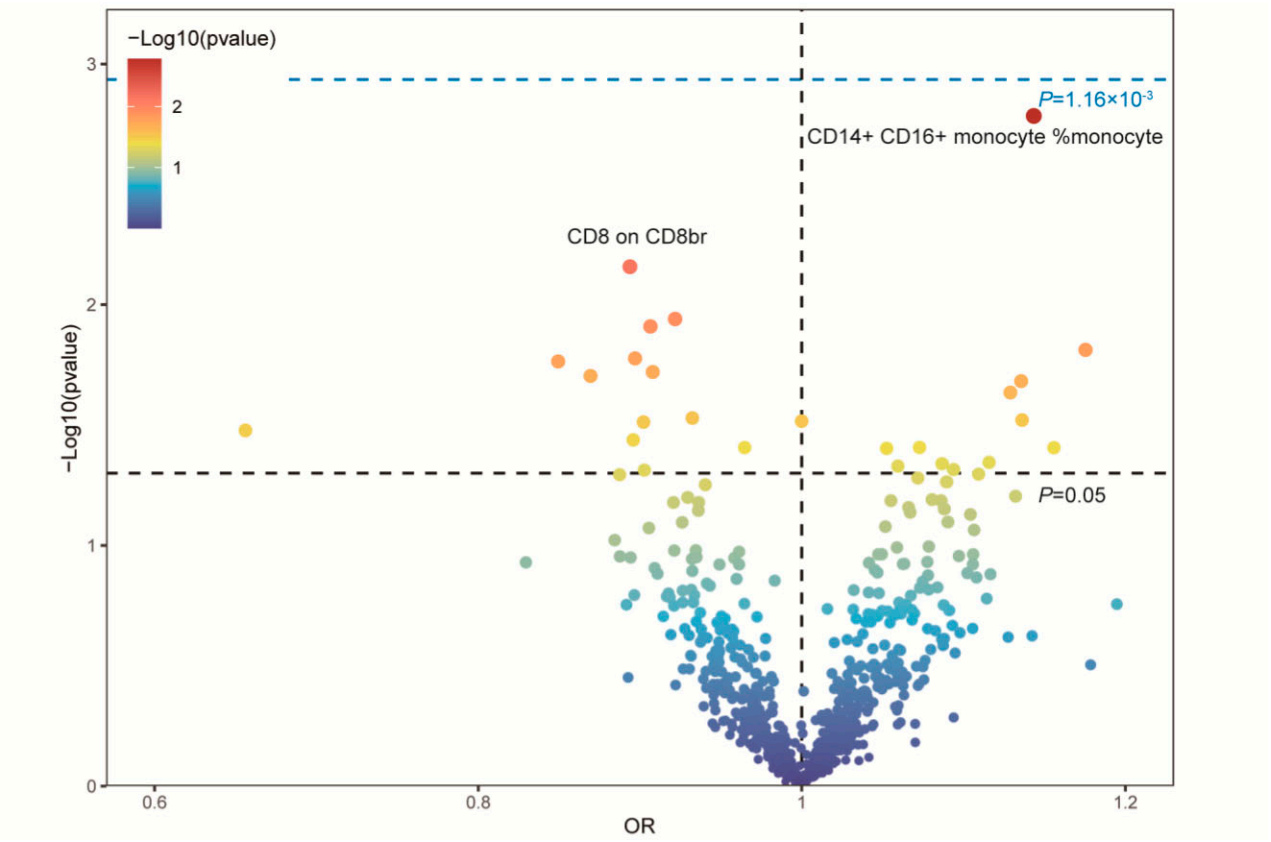

Figure 5: Forest plot and volcano plot indicating IVW analysis results of NS. (**a**) Forest plot demonstrating immunophenotypes with a positive causal relationship with NS. Beta = ln (OR), expressing as change in ln (OR) of outcome per each additional SD unit of exposure. (**b**) Volcano plots depicting causal associations of 731 immunophenotypes with NS. nSNP, number of SNPs; OR, odds ratio; CI, confidence interval.

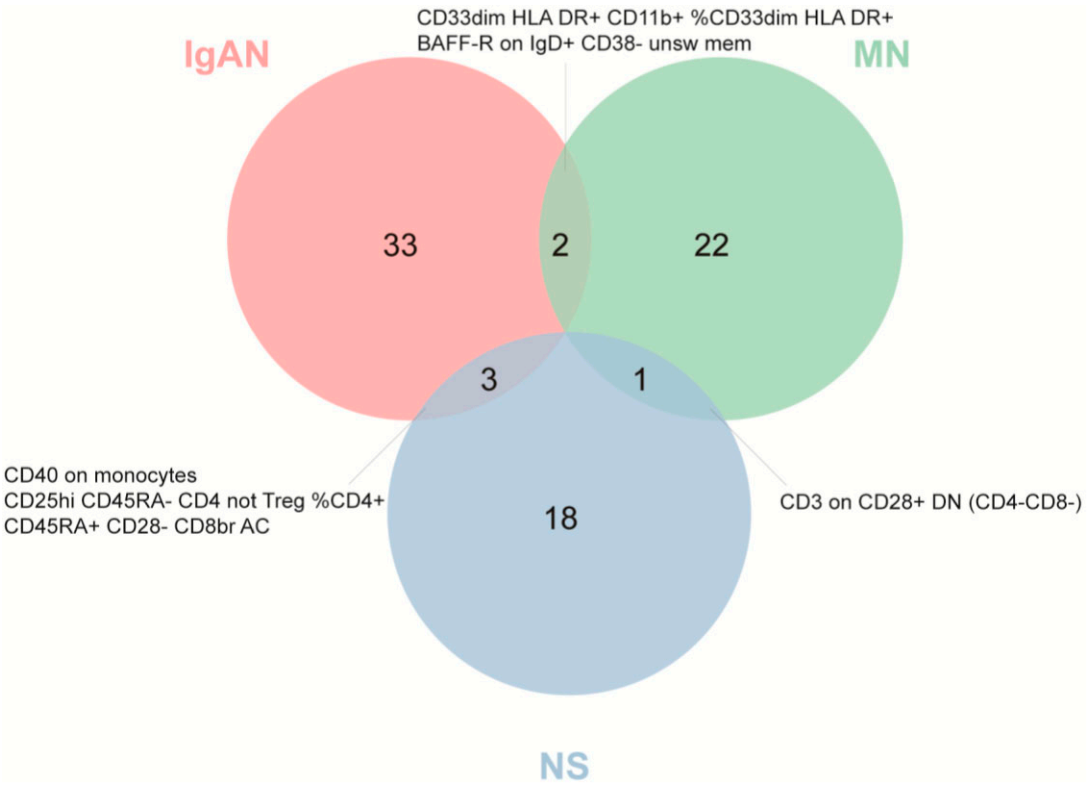

Figure 6: Venn diagram indicating common immunophenotypes across PGDs.

Kawasaki disease [12]. Increasing evidence also shows that CD40 activation is promising in cancer immunotherapy, leading to the development and clinical trials of CD40 agonists. Selicrelumab, the most studied CD40 agonist, has shown initial efficacy in neoadjuvant chemotherapy for pancreatic ductal adenocarcinoma (PDAC) in phase I trials [36, 37]. These findings suggest that CD40 agonists, like Selicrelumab, may also have therapeutic potential in IgAN and other autoimmune diseases from a genetic perspective.

Besides, we found that elevated CD64 expression on $CD14^+$ $CD16^-$ monocytes serves as a protective factor against IgAN. Classical monocytes, expressing $CD14^+$ and $CD16^-$, represent ~80%–85% of total monocytes, which undergo phagocytosis within tissues and are involved in the clearance of immune complexes [38, 39]. CD64, the only high-affinity IgG receptor in humans, is primarily expressed on monocytes, macrophages, and neutrophils [40]. By binding to the Fc region of IgG, CD64 enhances the phagocytosis of immune complexes by monocytes, including Kupffer cells, which play a predominant role in clearing IgA-containing immune complexes [41, 42]. Conversely, elevated CX3CR1 expression on monocytes is a risk factor for IgAN. CX3CR1, abundant on monocytes and macrophages, promotes adhesion and recruitment of monocytes, and is a marker for TGF-β production, a profibrotic mediator [43]. The CX3CR1-fractalkine axis has been linked to worsening hematuria, serum creatinine levels, and 24-hour urine protein levels in IgAN [44, 45]. Anti-CX3CR1 antibody treatment has shown significant reduction in glomeruli leukocyte filtration and prevention of crescent formation, suggesting that CX3CR1 exacerbates inflammation and fibrosis [46]. This evidence demonstrates that the role of monocytes in the pathogenesis of IgAN is complex, with different monocyte phenotypes having distinct effects on IgAN.

In this study, no immunophenotypes showed significant causal associations for MN and NS after applying Bonferroni correction. We consider that there are two potential reasons. First, the sample size of IgAN for the original GWAS is substantially larger than that of MN and NS, which enhances the significance, accuracy, and reliability of causal relationships [47]. Second, these results might reflect the fact that immune dysregulation is a more critical initiating factor for IgAN in terms of pathophysiology. Therefore, large-scale GWAS of PGDs, especially in MN and NS, through widespread collaborations to identify more associations and exploratory studies on immunophenotypes are needed to further explore the causal associations between immunophenotypes and PGDs.

Despite that no immunophenotypes demonstrated significant causal associations with MN and NS, we proceeded to explore common immune factors for PGDs by utilizing the suggestive immunophenotypes and constructing a Venn diagram. Four immunophenotypes play similar roles in PGDs (BAFF-R expression on IgD^+ $CD38^-$ unswitched memory B cells and the percentage of CD33dim HLA DR^+ $CD11b^+$ within CD33dim HLA DR^+ myeloid cell population for IgAN and MN; the percentage of CD25hi $CD45RA^-$ CD4 not Treg within $CD4^+$ T cell population for NS and IgAN; CD3 expression on $CD28^+$ DN for MN and IgAN), while one immune phenotype has opposite effects in PGD (CD40 expression on monocytes for IgAN and NS).

Previous studies have demonstrated that B cells play a significant role in the pathogenesis of PGDs [4, 8, 9]. We discovered that elevated levels of BAFF-R expression on IgD^+ $CD38^-$ unswitched memory B cells exert a protective effect against IgAN and MN occurrence. BAFF-R is a critical marker for the pro-survival B cells by binding to BAFF, which activates several downstream pathways that regulate basic survival functions including

protein synthesis and energy metabolism [48]. Recent studies have found that serum BAFF levels are increased in patients with IgAN and MN, which are associated with clinical and prognostic outcomes of the disease [49, 50]. However, our studies found that BAFF-R expressed on IgD^+ $CD38^-$ unswitched memory B cells exerts a protective effect. Researchers found that unswitched memory B cells were negatively correlated with levels of autoantibodies, and that the elevated levels of BAFF-R improve the survival of this subset and enhance their protective effects [51, 52].

Interestingly, we observed the elevated of CD40 expression on monocytes has opposite causal effects on IgAN (protective) and NS (risk). Studies have shown that CD40 monocytes are a pro-inflammatory subset that induce the activation, proliferation, and cytokine production of $CD4^+$ T cells [53]. Compared with other monocytes, CD40 monocytes express higher levels of inflammatory markers, thus enhancing the function of $CD4^+$ T cells [54]. It seems that CD40 expression on monocytes appears to be a risk factor for IgAN and NS. However, as discussed earlier, CD40 monocytes are a protective factor for IgAN by eliminating IgA1 [55]. The results prove that the pathogenic role of IgA1 outweighs the inflammatory contributions in IgAN.

As for MN and NS, elevated CD3 expression on $CD28^+$ DN ($CD4^-CD8^-$) is a risk factor. CD3 plays a significant role in T cell development and differentiation. The CD3–TCR complex serves as the initial signal for T cell activation, therefore an increase in CD3 indicates heightened T cell activity [29]. DN ($CD4^-CD8^-$) Tregs influence the immune system by secreting perforin and inducing cell apoptosis through the FAS–FASL pathway [56]. Numerous studies have shown that perforin induces the death of kidney cells and exacerbates kidney fibrosis [57, 58]. Although there is a lack of direct evidence on the causal association of DN Treg with MN and NS, we provide genetic evidence indicating that DN Treg is a risk factor for both diseases.

Despite its strengths, our studies also have some limitations. First, we used the standard $P < 10^{-5}$ instead of $P < 5 \times 10^{-8}$ when immunophenotypes and NS were used as the exposure, which may introduce some bias and false positives. Additionally, our GWAS data were derived exclusively from European populations, making the finding not generalizable to other populations. Therefore, in the future, with validation in larger populations and additional SNP analysis, we can clarify the causal association of immunophenotypes on PGDs more clearly and identify them as biomarkers in risk prediction, early detection, and prevention strategies in clinical settings.

CONCLUSION

In conclusion, our studies have uncovered causal relationships between 731 immunophenotypes and PGDs. We present direct genetic evidence, highlighting the crucial roles of specific immune cell phenotypes in the pathogenesis of PGDs. Notably, effector memory T cells and monocyte markers such as CD40, CD64, and CX3CR1 play a significant part in IgAN. Nevertheless, the precise mechanisms remain to be fully elucidated. Further experimentation and genetic investigations are imperative to understand the intricacies of PGDs. Additionally, our research offers invaluable immunological insights for PGDs, paving the way for future early clinical diagnosis and treatment approaches.

SUPPLEMENTARY DATA

Supplementary data are available at *Clinical Kidney Journal* online.

ACKNOWLEDGEMENTS

We extend our gratitude to the participants and investigators of the PGDs GWAS, immunophenotype GWAS, and GWAS Catalog project for making their data publicly available. Additionally, we would like to thank everyone involved in our study.

FUNDING

This study was funded by the National Key R&D Program of China (no. 2022YFC2705101), Chongqing Science and Health Joint Medical Research Project (grant no. 2023GGXM001), and Program for Youth Innovation in Future Medicine, and Chongqing Medical University (no. W0098).

AUTHORS' CONTRIBUTIONS

Conceptualization was done by X.Y. and W.T. Data curation, formal analysis, and visualization were the responsibility of W.T. and X.Y. Funding acquisition and supervision were done by H.Y. and Q.L. Investigation, methodology, and resources were organized by W.T. and X.Y. Project administration was done by X.Y., H.Y., and Q.L. Software was written by W.T. and X.Y. The original draft was written by W.T. Review and editing of the manuscript was done by X.Y., H.Y., and Q.L. All authors read and approved the final manuscript.

DATA AVAILABILITY STATEMENT

The original contributions presented in the study are included in the article and supplementary material. Further inquiries can be directed to the corresponding author.

CONFLICT OF INTEREST STATEMENT

The authors declare no potential conflict of interest.

ETHICS STATEMENT

All data for this study were sourced from previously published research and public databases, which were obtained with relevant participant consent and ethical approval.

REFERENCES

1. Hricik DE, Chung-Park M, Sedor JR. Glomerulonephritis. *N Engl J Med* 1998;**339**:888–99. https://doi.org/10.1056/NEJM199809243391306
2. Kalantar-Zadeh K, Jafar TH, Nitsch D *et al*. Chronic kidney disease. *Lancet* 2021;**398**:786–802. https://doi.org/10.1016/S0140-6736(21)00519-5
3. Wyatt RJ, Julian BA. IgA nephropathy. *N Engl J Med* 2013;**368**:2402–14. https://doi.org/10.1056/NEJMra1206793
4. Stamellou E, Seikrit C, Tang SCW *et al*. IgA nephropathy. *Nat Rev Dis Primers* 2023;**9**:67. https://doi.org/10.1038/s41572-023-00476-9
5. Cheung CK, Barratt J, Lafayette R *et al*. Targeting APRIL in the treatment of glomerular diseases. *Kidney Int* 2024;**106**:806–18 https://doi.org/10.1016/j.kint.2024.08.012
6. Lin YC, Gau TS, Jiang ZH *et al*. Targeted therapy in glomerular diseases. *J Formos Med Assoc* 2024;**123**:149–58. https://doi.org/10.1016/j.jfma.2023.06.020

7. Gentile M, Sanchez-Russo L, Riella LV *et al*. Immune abnormalities in IgA nephropathy. *Clin Kidney J* 2023;**16**:1059–70. https://doi.org/10.1093/ckj/sfad025
8. Vivarelli M, Gibson K, Sinha A *et al*. Childhood nephrotic syndrome. *Lancet* 2023;**402**:809–24. https://doi.org/10.1016/S0140-6736(23)01051-6
9. Ronco P, Beck L, Debiec H *et al*. Membranous nephropathy. *Nat Rev Dis Primers* 2021;**7**:69. https://doi.org/10.1038/s41572-021-00303-z
10. Emdin CA, Khera AV, Kathiresan S. Mendelian randomization. *JAMA* 2017;**318**:1925–6. https://doi.org/10.1001/jama.2017.17219
11. Tin A, Köttgen A. Mendelian randomization analysis as a tool to gain insights into causes of diseases: a primer. *J Am Soc Nephrol* 2021;**32**:2400–7. https://doi.org/10.1681/ASN.2020121760
12. Orrù V, Steri M, Sidore C *et al*. Complex genetic signatures in immune cells underlie autoimmunity and inform therapy. *Nat Genet* 2020;**52**:1036–45. https://doi.org/10.1038/s41588-020-0684-4
13. Kiryluk K, Sanchez-Rodriguez E, Zhou XJ *et al*. Genome-wide association analyses define pathogenic signaling pathways and prioritize drug targets for IgA nephropathy. *Nat Genet* 2023;**55**:1091–105. https://doi.org/10.1038/s41588-023-01422-x
14. Sakaue S, Kanai M, Tanigawa Y *et al*. A cross-population atlas of genetic associations for 220 human phenotypes. *Nat Genet* 2021;**53**:1415–24. https://doi.org/10.1038/s41588-021-00931-x
15. Xie J, Liu L, Mladkova N *et al*. The genetic architecture of membranous nephropathy and its potential to improve non-invasive diagnosis. *Nat Commun* 2020;**11**:1600. https://doi.org/10.1038/s41467-020-15383-w
16. Skrivankova VW, Richmond RC, Woolf BAR *et al*. Strengthening the reporting of observational studies in epidemiology using mendelian randomisation (STROBE-MR): explanation and elaboration. *BMJ* 2021;**375**:n2233. https://doi.org/10.1136/bmj.n2233
17. Wang X, Cheng H, Feng M *et al*. Causality of genetically proxied immunophenotypes on cardiovascular diseases: a Mendelian randomization study. *Front Immunol* 2024;**15**:1344773. https://doi.org/10.3389/fimmu.2024.1344773
18. Brion MJ, Shakhbazov K, Visscher PM. Calculating statistical power in Mendelian randomization studies. *Int J Epidemiol* 2013;**42**:1497–501. https://doi.org/10.1093/ije/dyt179
19. Jiang L, Li JC, Tang BS *et al*. Associations between gut microbiota and Parkinson disease: a bidirectional Mendelian randomization analysis. *Euro J Neurology* 2023;**30**:3471–7. https://doi.org/10.1111/ene.15848
20. Burgess S, Butterworth A, Thompson SG. Mendelian randomization analysis with multiple genetic variants using summarized data. *Genet Epidemiol* 2013;**37**:658–65. https://doi.org/10.1002/gepi.21758
21. Bowden J, Davey Smith G, Haycock PC *et al*. Consistent estimation in Mendelian randomization with some invalid instruments using a weighted median estimator. *Genet Epidemiol* 2016;**40**:304–14. https://doi.org/10.1002/gepi.21965
22. Bowden J, Davey Smith G, Burgess S. Mendelian randomization with invalid instruments: effect estimation and bias detection through Egger regression. *Int J Epidemiol* 2015;**44**:512–25. https://doi.org/10.1093/ije/dyv080
23. Verbanck M, Chen CY, Neale B *et al*. Publisher correction: Detection of widespread horizontal pleiotropy in causal relationships inferred from Mendelian randomization between complex traits and diseases. *Nat Genet* 2018;**50**:1196. https://doi.org/10.1038/s41588-018-0164-2
24. Shu J, Ge Y, Wu Y. Causal role of immune cells in IgA nephropathy: a Mendelian randomization study. *Ren Fail* 2024;**46**:2381593. https://doi.org/10.1080/0886022X.2024.2381593
25. Seddiki N, Santner-Nanan B, Martinson J *et al*. Expression of interleukin (IL)-2 and IL-7 receptors discriminates between human regulatory and activated T cells. *J Exp Med* 2006;**203**:1693–700. https://doi.org/10.1084/jem.20060468
26. Narsale A, Moya R, Davies JD. Human CD4(+) CD25(+) CD127(hi) cells and the Th1/Th2 phenotype. *Clin Immunol* 2018;**188**:103–12. https://doi.org/10.1016/j.clim.2018.01.003
27. Esteve Cols C, Graterol Torres FA, Quirant Sánchez B *et al*. Immunological pattern in IgA nephropathy. *Int J Mol Sci* 2020;**21**:1389. https://doi.org/10.3390/ijms21041389
28. Schamel WW, Alarcon B, Minguet S. The TCR is an allosterically regulated macromolecular machinery changing its conformation while working. *Immunol Rev* 2019;**291**:8–25. https://doi.org/10.1111/imr.12788
29. van der Merwe PA, Dushek O. Mechanisms for T cell receptor triggering. *Nat Rev Immunol* 2011;**11**:47–55. https://doi.org/10.1038/nri2887
30. Smith-Garvin JE, Koretzky GA, Jordan MS. T cell activation. *Annu Rev Immunol*. 2009;**27**:591–619. https://doi.org/10.1146/annurev.immunol.021908.132706
31. Ruszkowski J, Lisowska KA, Pindel M *et al*. T cells in IgA nephropathy: role in pathogenesis, clinical significance and potential therapeutic target. *Clin Exp Nephrol* 2019;**23**:291–303. https://doi.org/10.1007/s10157-018-1665-0
32. Yang L, Zhang X, Peng W *et al*. MicroRNA-155-induced T lymphocyte subgroup drifting in IgA nephropathy. *Int Urol Nephrol* 2017;**49**:353–61. https://doi.org/10.1007/s11255-016-1444-3
33. Sun Q, Zhang J, Zhou N *et al*. DNA methylation in Cosmc promoter region and aberrantly glycosylated IgA1 associated with pediatric IgA nephropathy. *PLoS ONE* 2015;**10**:e0112305. https://doi.org/10.1371/journal.pone.0112305
34. Bai J, Wu Q, Chen J *et al*. Risk factors for recurrent IgA nephropathy after renal transplantation: a meta-analysis. *Biomol Biomed* 2023;**23**:364–75.
35. Dinoto A, Ferrari S, Mariotto S. Treatment options in refractory autoimmune encephalitis. *CNS Drugs* 2022;**36**:919–31. https://doi.org/10.1007/s40263-022-00943-z
36. Zhou Y, Richmond A, Yan C. Harnessing the potential of CD40 agonism in cancer therapy. *Cytokine Growth Factor Rev* 2024;**75**:40–56. https://doi.org/10.1016/j.cytogfr.2023.11.002
37. Byrne KT, Betts CB, Mick R *et al*. Neoadjuvant selicrelumab, an agonist CD40 antibody, induces changes in the tumor microenvironment in patients with resectable pancreatic cancer. *Clin Cancer Res* 2021;**27**:4574–86. https://doi.org/10.1158/1078-0432.CCR-21-1047
38. Bumbea V, Ardelean L, Radulescu L *et al*. Proinflammatory role of monocytes in SARS-CoV-2 infection in chronic hemodialysis patients. *Front Immunol* 2023;**14**:1210961. https://doi.org/10.3389/fimmu.2023.1210961
39. Clarkson SB, Kimberly RP, Valinsky JE *et al*. Blockade of clearance of immune complexes by an anti-Fc gamma receptor monoclonal antibody. *J Exp Med* 1986;**164**:474–89. https://doi.org/10.1084/jem.164.2.474
40. Mancardi DA, Albanesi M, Jönsson F *et al*. The high-affinity human IgG receptor FcγRI (CD64) promotes IgG-mediated inflammation, anaphylaxis, and antitumor

immunotherapy. *Blood* 2013;**121**:1563–73. https://doi.org/10.1182/blood-2012-07-442541
41. Nimmerjahn F, Ravetch JV. Fcgamma receptors as regulators of immune responses. *Nat Rev Immunol* 2008;**8**:34–47. https://doi.org/10.1038/nri2206
42. Chen A, Yang SS, Lin TJ *et al*. IgA nephropathy: clearance kinetics of IgA-containing immune complexes. *Semin Immunopathol* 2018;**40**:539–43. https://doi.org/10.1007/s00281-018-0708-7
43. Helmke A, Nordlohne J, Balzer MS *et al*. CX3CL1-CX3CR1 interaction mediates macrophage-mesothelial cross talk and promotes peritoneal fibrosis. *Kidney Int* 2019;**95**:1405–17. https://doi.org/10.1016/j.kint.2018.12.030
44. Cox SN, Sallustio F, Serino G *et al*. Activated innate immunity and the involvement of CX3CR1-fractalkine in promoting hematuria in patients with IgA nephropathy. *Kidney Int* 2012;**82**:548–60. https://doi.org/10.1038/ki.2012.147
45. Luo R, Guo SM, Li YQ *et al*. Plasma fractalkine levels are associated with renal inflammation and outcomes in immunoglobulin A nephropathy. *Nephrol Dial Transplant* 2019;**34**:1549–58. https://doi.org/10.1093/ndt/gfy169
46. Feng L, Chen S, Garcia GE *et al*. Prevention of crescentic glomerulonephritis by immunoneutralization of the fractalkine receptor CX3CR1 rapid communication. *Kidney Int* 1999;**56**:612–20. https://doi.org/10.1046/j.1523-1755.1999.00604.x
47. Visscher PM, Wray NR, Zhang Q *et al*. 10 Years of GWAS discovery: biology, function, and translation. *Am Hum Genet* 2017;**101**:5–22. https://doi.org/10.1016/j.ajhg.2017.06.005
48. Smulski CR, Eibel H. BAFF and BAFF-receptor in B cell selection and survival. *Front Immunol* 2018;**9**:2285. https://doi.org/10.3389/fimmu.2018.02285
49. Xin G, Shi W, Xu LX *et al*. Serum BAFF is elevated in patients with IgA nephropathy and associated with clinical and histopathological features. *J Nephrol* 2013;**26**:683–90. https://doi.org/10.5301/jn.5000218
50. Han SS, Yang SH, Jo HA *et al*. BAFF and APRIL expression as an autoimmune signature of membranous nephropathy. *Oncotarget* 2018;**9**:3292–302. https://doi.org/10.18632/oncotarget.23232
51. Castleman MJ, Santos AL, Lesteberg KE *et al*. Activation and pro-inflammatory cytokine production by unswitched memory B cells during SARS-CoV-2 infection. *Front Immunol* 2023;**14**:1213344. https://doi.org/10.3389/fimmu.2023.1213344
52. Vincent FB, Saulep-Easton D, Figgett WA *et al*. The BAFF/APRIL system: emerging functions beyond B cell biology and autoimmunity. *Cytokine Growth Factor Rev* 2013;**24**:203–15. https://doi.org/10.1016/j.cytogfr.2013.04.003
53. Karnell JL, Rieder SA, Ettinger R *et al*. Targeting the CD40-CD40L pathway in autoimmune diseases: humoral immunity and beyond. *Adv Drug Deliv Rev* 2019;**141**:92–103. https://doi.org/10.1016/j.addr.2018.12.005
54. Yang J, Fang P, Yu D *et al*. Chronic kidney disease induces inflammatory $CD40^+$ monocyte differentiation via homocysteine elevation and DNA hypomethylation. *Circ Res* 2016;**119**:1226–41. https://doi.org/10.1161/CIRCRESAHA.116.308750
55. Rifai A, Mannik M. Clearance of circulating IgA immune complexes is mediated by a specific receptor on Kupffer cells in mice. *J Exp Med* 1984;**160**:125–37. https://doi.org/10.1084/jem.160.1.125
56. Ligocki AJ, Niederkorn JY. Advances on Non-CD4 + $Foxp3^+$ T regulatory cells: $CD8^+$, Type 1, and double negative T regulatory cells in organ transplantation. *Transplantation* 2015;**99**:1553–9. https://doi.org/10.1097/TP.0000000000000813
57. Sharma VK, Bologa RM, Li B *et al*. Molecular executors of cell death—differential intrarenal expression of Fas ligand, Fas, granzyme B, and perforin during acute and/or chronic rejection of human renal allografts. *Transplantation* 1996;**62**:1860–6. https://doi.org/10.1097/00007890-199612270-00031
58. Hao J, Huang X, Guan J *et al*. Shenkang injection protects against renal fibrosis by reducing perforin expression through the STING/TBK1/IRF3 signaling pathways in natural killer cells. *Phytomedicine* 2022;**104**:154206. https://doi.org/10.1016/j.phymed.2022.154206

Received: 10.10.2024; Editorial decision: 28.1.2025